Article

Effect of Polymeric Binders on Dispersion of Active Particles in Aqueous LiFePO₄-Based Cathode Slurries as well as on Mechanical and Electrical Properties of Corresponding Dry Layers

Ronald Gordon,* Meriem Kassar, and Norbert Willenbacher

Read Online

ACCESS | Metrics & More | Article Recommendations | Supporting Information

ABSTRACT: We investigated the effect of carboxymethyl cellulose (CMC) and the particulate fluorine/acrylate hybrid polymer (FAHP) on the flow behavior of LiFePO₄-based cathode slurries as well as on electrical and mechanical properties of the corresponding dry layers. CMC dissolves in water and partly adsorbs on the active particles. Thus, it has a strong impact on particle dispersion and a critical CMC concentration distinguished by a minimum in yield stress and high shear viscosity is found, indicating an optimum state of particle dispersion. In contrast, the nanoparticulate FAHP binder has no effect on slurry rheology. The electrical conductivity of the dry layer exhibits a maximum at a CMC concentration corresponding to the minimum in slurry viscosity but monotonically decreases with increasing FAHP concentration. Adhesion to the current collector is provided by FAHP, and the line load in peel tests strongly increases with FAHP concentration, whereas CMC does not contribute to adhesion. The electrical conductivity and adhesion values obtained here excel reported values for similar aqueous LiFePO₄-based cathode layers using alternative polymeric binders. Both CMC and FAHP contribute to the cohesive strength of the layers; the contribution of CMC, however, is stronger than that of FAHP despite its lower intrinsic mechanical strength. We attribute this to its impact on the cathode microstructure since high CMC concentrations result in a strong alignment of LiFePO₄ particles, which yields superior cohesive strength.
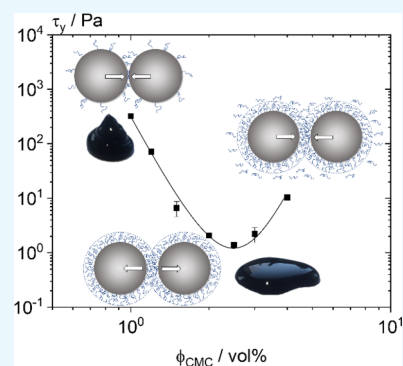
1. INTRODUCTION

Lithium iron phosphate (LiFePO₄) has been extensively investigated for over two decades since it was reported as a potential cathode material for lithium-ion batteries (LiB).[1] Its high theoretical capacity (170 mA h g⁻¹), stability during charge/discharge, thermal stability, low cost and toxicity, and its environmental compatibility as well as its safety make it a suitable cathode active material for large cell applications.[1−6] However, poor electrical conductivity (10^{-9} S cm⁻¹) and a low Li⁺-ion diffusion coefficient (1.8×10^{-18} m² s⁻¹) at room temperature represent intrinsic drawbacks for LiFePO₄ as a battery cathode material.[7−9] Therefore, considerable research work dealt with the improvement of ionic and electronic conductivity through decrease of particle size, addition of carbon, or ion doping.[10−17] Although the former concept has improved cell performance, agglomeration of LiFePO₄ fine particles still constitutes a problem during processing of cathode slurries and limits electrochemical performance of corresponding electrodes.

Conventionally, organic solvents, such as *N*-methyl-2-pyrrolidone (NMP), are used for dispersing active materials and dissolving polymeric additives for control of processing behavior of the slurry during cathode manufacturing as well as to improve mechanical properties of the dry layer.[18−20] These solvents are not only environmentally harmful but also toxic,

flammable, and expensive. Hence, water-based electrodes have been developed as greener alternative. Several research activities concentrated on exploring novel aqueous binder systems for LiFePO₄-based cathodes such as polyacrylic acid (PAA),[21−23] chitosan and its derivatives (CTS, CCTS, CN-CCTS),[24−27] poly(4-styrene sulfonic acid) (PSSA),[28] styrene butadiene rubber (SBR),[22] poly(vinyl acetate) (PVAc),[8] polytetrafluorethylene (PTFE),[29] and xanthan,[30] as well as lithium and sodium salts of carboxymethyl cellulose (LiCMC, NaCMC).[31−38]

Carboxymethyl cellulose (CMC) and SBR are often combined as polymeric binders. CMC is a linear, long-chain, anionic polysaccharide, consisting of two anhydroglucose units with three hydroxyl groups each, enabling its solubility in water. SBR is not soluble in water and is thus added as nanoparticulate dispersion to the slurry. Li and Lin studied the interaction between organic additives and active materials and the resulting electrochemical performance of corresponding
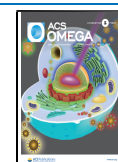
cells.[36] Zeta potential and sedimentation measurements of LiFePO$_4$ and carbon black (CB) showed that both dispersed SBR particles and molecularly dissolved CMC can adsorb on the solid particles. SBR showed higher affinity than CMC to adsorb on the LiFePO$_4$ particle surface. Nevertheless, CMC, as a dissociable polyelectrolyte, provided a superior effect on the dispersion of solid particles through electrosteric stabilization.

Instead of SBR, particulate FAHP has been blended with CMC for manufacturing water-based cathodes.[39−43] These reported studies improved coating surface quality and higher adhesive strength between the cathode layer and current collector when increasing FAHP concentration. In addition, electrodes based on FAHP show high thermal stability and equivalent electrochemical performance compared to conventionally fabricated NMP-based cathodes. Still, the influence of FAHP on the performance of LiFePO$_4$-based cathodes has not been addressed yet.

Binder properties and concentration affect not only the dispersion behavior of solid particles but also the resulting electrical conductivity of the electrode. Even though the addition of CB particles reduces the electrical resistivity in the electrode layer, particle agglomeration leads to discontinuous conductive pathways. The addition of dispersing polymeric binders at appropriate concentrations and particle to binder ratios results in homogeneous particle distribution and formation of a conducting network, enhancing electron transport kinetics.[44−47] As a result, the rate capability of the electrode can be improved, yielding higher cell energy and power as well as enhanced battery lifetime. Furthermore, polymeric binders are of utmost importance for the mechanical integrity of the electrode, determining battery lifetime. The electrode must withstand mechanical stresses due to expansion and shrinkage of the electrochemically active material during charge/discharge cycles.[48,49] These volume fluctuations can result in delamination of the electrode layer from the current collector and cracking within the layer. Therefore, the determination and improvement of adhesive strength between the layer and collector have been thoroughly investigated.[27,50−54] However, the cohesive strength in the electrode layer has not received much attention. Indentation, tensile, scratch, and drag tests have been used to characterize the mechanical strength of electrode layers.[54−61] Despite several efforts to bring light into how mechanical properties depend on formulation and slurry processing, the complex contribution of the binder to the processing behavior, mechanical strength, microstructure, and electrochemical performance of LiB cathodes still needs an in-depth investigation. In preliminary work, we demonstrated that the intrinsic cohesive strength of electrode layers can be characterized using standard methods for mechanical characterization such as compression, flexural, tensile, and torsion tests using samples of sufficient thickness. In the present work, the cohesive strength of cathode layers is characterized by employing compression tests.

In this study, we first investigate the interaction of CMC and FAHP with LiFePO$_4$ and CB particles, using rheological data of cathode slurries to understand the polymer adsorption behavior. The electrical conductivity of dry cathode layers is determined and correlated to the flow behavior of corresponding slurries to elucidate the relationship between polymer adsorption and component distribution. Moreover, adhesive strength measurements and, for the first time, data regarding the cohesive strength of LiFePO$_4$-based cathodes are

presented. Finally, the effect of the polymeric binders on the cathode microstructure is studied and linked to the cohesive strength.

2. EXPERIMENTAL SECTION

2.1. Materials. Needle-shaped LiFePO$_4$ (LFP) particles (Tatung Fine Chemicals Co., Taiwan) with a carbon coating of 1.5 wt %, a density of 3.5 g cm^{-3}, a specific surface area S_A of 11.3 m^{2}g^{-1}, and an equivalent sphere, volume-based average diameter $x_{50,3}$ of 2.8 μm were used as an active material. Carbon black (CB, Alfa Aesar, United States) with a density of 1.73 g cm^{-3} and a specific surface area S_A of 70.3 m^2 g^{-1} was added as a conductivity promoter. According to the manufacturer, the CB particles have a primary particle size $x_{50,3}$ of 42 nm. However, they agglomerate, reaching an average diameter of 5 μm as determined by Fraunhofer diffraction (HELOS H0309, Sympatec GmbH, Germany) equipped with an ultrasonic dispersing unit (QUIXEL, Sympatec GmbH, Germany) used to disperse the particles in ethanol. Carboxymethyl cellulose (Sigma-Aldrich, Germany) with a molecular weight M_w of 700 kDa and a degree of substitution DS of 0.9 was used as a binder. In addition, an aqueous suspension of 41 wt % fluorine/acrylate hybrid polymer (FAHP; TRD202A, JSR Micro NV., Belgium) with a particle size of 200 nm, a density of 1.2 g cm^{-3}, and a glass transition temperature of −5 °C, corresponding to the maximum of the loss modulus G″ (Figure 1), was added to improve the
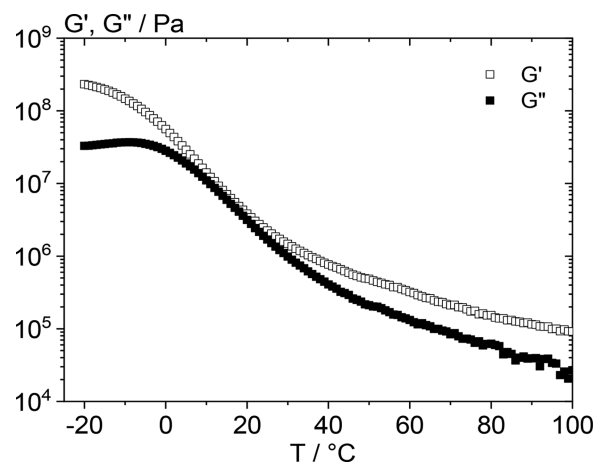
Figure 1. Storage (G′) and loss (G″) modulus of FAHP as a function of temperature. Measurements were performed at a constant deformation γ of 0.01% and a frequency f of 0.1 Hz using films of 0.9 mm height.

mechanical strength of the cathode layer. Small-amplitude oscillatory shear experiments (Figure 1) at fixed frequency covering a broad temperature range from −20 to 100 °C on dry FAHP films did not show a cross-over of the storage (G′) and loss (G″) moduli in the high-temperature range, indicating a high molecular weight of the polymer or even chemical cross-linking. Gravimetric measurements using toluene as solvent yielded a degree of cross-linking of 84.1 ± 3.4%.

2.2. Sample Preparation. Water-based cathode slurries were prepared at constant mixing conditions with a total solids volume fraction ϕ_p of 24 vol % at an LFP to carbon black mass ratio of 48:1. The CMC concentration was varied between 1 and 8 vol % referring to the dry electrode layer. First, CMC was dissolved and homogenized in 80% of the total amount of

water needed for the slurry using a 55 mm propeller mixing geometry at 1200 rpm for 25 min. LFP followed by CB was dispersed in the CMC solution using a 50 mm dissolver disk at 2000 rpm for 35 min each. Finally, the remaining amount of water was added and mixed at 2000 rpm for 5 min. For slurries containing FAHP as the secondary binder, the polymer suspension was added to the slurry directly after preparing the CMC solution and was homogenized at 1200 rpm for 10 min.

Slurries were coated on glass plates and aluminum foil for electrical conductivity and adhesive strength measurements, respectively, using a doctor blade (ZUA 2000, Zehntner GmbH, Switzerland) with a coating width of 60 mm and a coating gap of 300 μm. The wet films were dried at 80 °C for 30 min and then cut into 25 mm width and 60 mm length specimens for the adhesive strength test. To obtain samples for cohesive strength testing, slurries were poured into a 26 mm × 49 mm × 11 mm (W×L×H) silicone mold and dried at 80 °C overnight. Subsequently, the dry layers were cut and grinded into samples of 2 mm width, 5 mm length and 5 mm height. Sandpaper with rough texture was used to shape the samples and fine sandpaper was applied to smooth the edges.

2.3. Sample Characterization. *2.3.1. Rheological Measurements.* Rotational steady shear measurements were carried out using a shear stress-controlled rheometer (Physica, MCR 501, Anton Paar GmbH, Germany) equipped with a 25 mm plate-plate geometry. The shear stress-dependent viscosity $\eta(\tau)$ and the yield stress τ_y were determined by applying a stepwise, logarithmic shear stress ramp in the range $\tau = 0.1$ Pa to $\tau = 1000$ Pa at a gap width of 1 mm. The yield stress τ_y was determined using the tangent intersection point method.[62,63] The critical stress at which the tangents applied to the linear and flow region of the stress-dependent deformation curve cross is defined as τ_y. All measurements were performed at 20 °C.

2.3.2. Electrical Conductivity Tests. The four-point resistivity test was conducted using a customized setup equipped with four equally spaced measuring probes (S4D5G, Uwe Electronic GmbH, Germany). Five different currents were applied at three different positions of the 60 mm × 120 mm electrode layer. The corresponding voltage was used to calculate the average electrical conductivity according to Smits.[64]

2.3.3. Mechanical Properties. Mechanical tests were carried out using a universal testing machine (Texture Analyzer, TA.XT plus, Stable Micro Systems, UK) equipped with a 5 kg load cell force sensor (max. force of 50 N, force sensitivity of 1 mN).

The adhesive strength of electrode layers to aluminum foil was investigated employing 90° peel tests based on the standard DIN 28510-1. Therefore, electrode layers with a film thickness between 80 and 100 μm were fixed to a measuring plate with the help of double-sided adhesive tape (Universal, Tesa SE., Germany). Subsequently, a 500 g plate was set on top of the electrode layer as a precompression step and removed before the measurement to ensure homogeneous contact between adhesive tape and layer. Measurements were performed at a constant peel velocity of 5 mm s^{-1}, and the measured tensile force F was expressed as line load F/25 mm, characterizing the adhesive strength.

The cohesive strength of thick electrode samples was studied using the compression test based on the standard DIN 51104. Samples were compressed using a steel plate at a constant

velocity of 1 mm s^{-1} until reaching the breaking point of the samples. Hereby, the maximum compression stress prior to failure $\sigma_{c,max}$ was used to characterize the cohesive strength in the electrode layer. In addition, tensile tests for pure polymers films were carried out at 20 °C based on the standard DIN ISO EN 527-4.
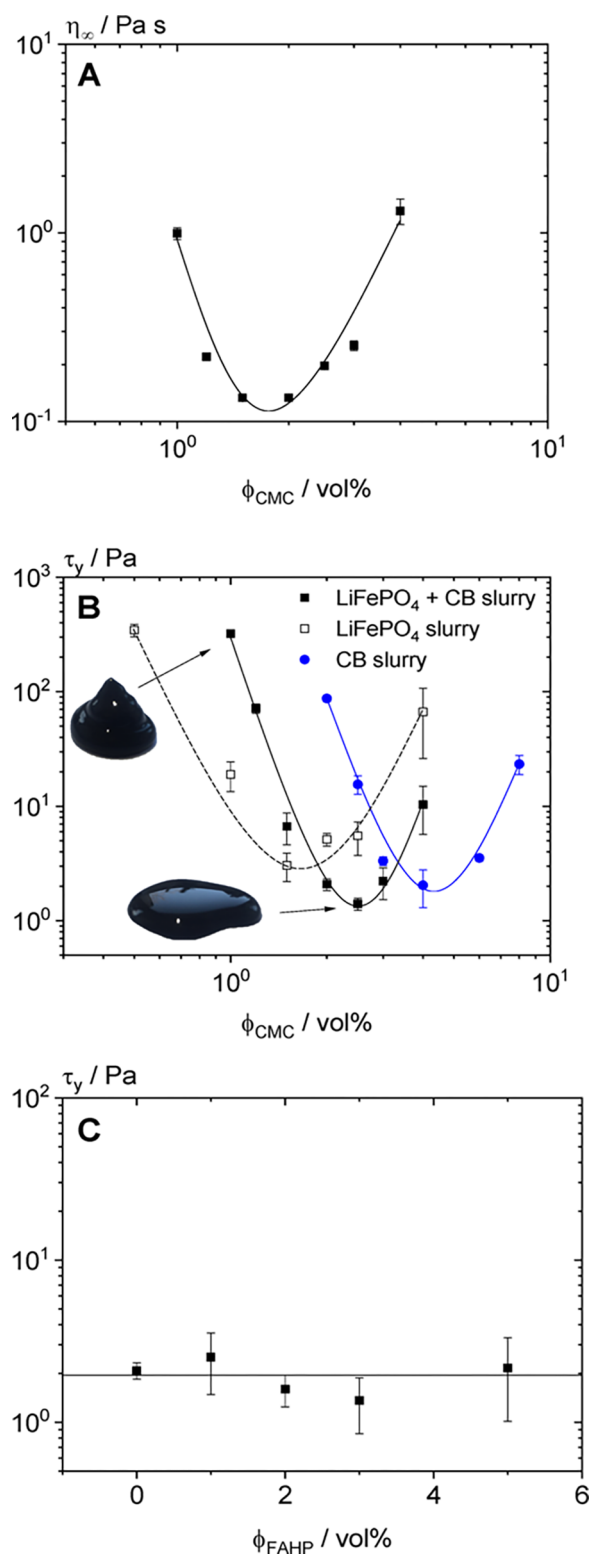
2.3.4. Microstructure. The porosity of electrode layers was determined based on the Archimedes density according to the standards DIN 993-1 and DIN 993-18. Additionally, cross-sectional images of vacuum-infused electrode layers were investigated by means of scanning electron microscopy (SEM) using a LEO1530 microscope (Carl Zeiss AG, Oberkochen, Germany) to characterize their microstructure, particularly the orientation distribution of the needle-shaped LiFePO$_4$ particles.

3. RESULTS AND DISCUSSION

3.1. Rheological Characterization of Cathode Slurries. The flow behavior of suspensions well below the maximum packing fraction of the particles is controlled by the viscosity of the dispersed phase, the solvent viscosity η_s, the particle volume fraction ϕ_p, and size and shape of the particles as well as the interparticle interactions. When attractive particle interactions dominate, the suspensions may exhibit a yield stress τ_y. The absolute value of this quantity is determined by the strength of particle attraction and the number of particle contacts as well as particle size. The high shear limiting viscosity $\eta(\dot{\gamma} \rightarrow \infty) = \eta_\infty$, i.e., when hydrodynamic interactions dominate over thermodynamic particle interactions, solely depends on ϕ_p and η_s. The latter parameter is governed by the type and amount of dissolved polymer. Accordingly, rheological data of LiFePO$_4$/CB slurries with varying amounts of added CMC provide insight into the adsorption of the CMC molecules on the particle surface. The fraction of CMC adsorbed on the particles provides steric repulsion superimposing with van der Waals attraction forces and thus affects τ_y. The part of CMC molecularly dissolved in the dispersed phase contributes to η_s and hence η_∞.

In the present study, rheological data is used to characterize the influence of CMC on dispersion of LiFePO$_4$ and CB particles in the slurry. Steady shear measurements were carried out to study the flow behavior of cathode slurries at a constant solid volume fraction ϕ_p of 24 vol % and a fixed LiFePO$_4$ to CB ratio 48:1 but varying the CMC concentration ϕ_{CMC}. The viscosity $\eta(\dot{\gamma})$ of cathode slurries decreases with the increasing CMC amount, reaching a minimum at a critical concentration and increases upon further addition of CMC (see the Supporting Information).

This effect can be observed more clearly by plotting the high shear viscosity $\eta_\infty = \eta(\dot{\gamma} = 800$ s$^{-1})$ against ϕ_{CMC} as shown in Figure 2A. The high shear viscosity exhibits a pronounced minimum as a function of CMC concentration. This can be rationalized as follows: Without CMC or at low CMC concentration, van der Waals attraction among particles dominates and aggregates are formed, which are stable even when exposed to high shear forces. These aggregates immobilize part of the solvent, and hence, the effective particle volume fraction exceeds ϕ_p and this results in high values of η_∞. As more and more CMC adsorbs on the particles, electrosteric repulsion partly prevents aggregation, and thus, η_∞ decreases until the particles are fully dispersed or the particle surfaces are saturated with CMC. Further addition of CMC then leads to an increase in η_∞ due to the contribution
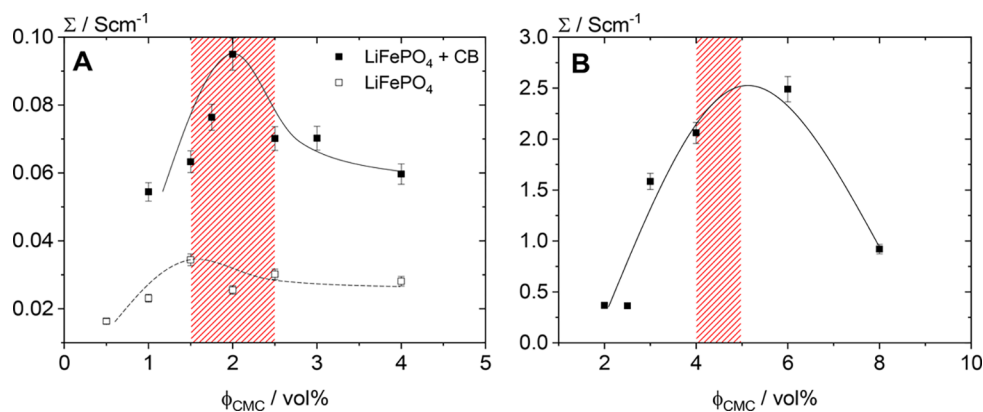
of the dissolved polymer to the viscosity of the continuous phase η_s. Our results demonstrate that in the investigated cathode slurries, CMC acts as a dispersing agent at low concentration but as a thickener at high polymer fraction. Note, a nonadsorbing polymer would cause a monotonic increase in η_∞ with increasing polymer concentration as a result of a progressive enhancement of η_s. A similar change in rheological properties upon addition of CMC was observed for graphite-based LiB anode slurries.[65] However, the implications of this effect on further electrode properties were not discussed.

The adsorption of CMC on the active material and conductive agent particle surface and hence its impact on particle dispersion also show up in the yield stress of the slurry, i.e., the stress at which plastic deformation starts. Slurries comprising only LiFePO$_4$ or CB were investigated to systematically understand the adsorption behavior of CMC on both particle species. Figure 2B displays the yield stress as a function of ϕ_{CMC} for LiFePO$_4$- and CB-based slurries as well as cathode slurries including both components. Note, slurries containing only CB as solid particles were characterized at a constant solid volume fraction ϕ_p of 3.5 vol %. All slurries exhibit a pronounced minimum in τ_y vs. ϕ_{CMC}, and the yield stress drops by about two orders of magnitude. The yield stress in such slurries is a signature of a percolating particle network self-assembling due to the predominantly attractive particle interactions; its absolute value is determined by the strength of the attractive force and the number of particle contacts per volume. The initial decrease of τ_y with increasing ϕ_{CMC} is a consequence of the increasing electrosteric repulsion among particles due to the adsorbed CMC partially compensating the strong van der Waals attraction. The minimum of the τ_y (ϕ_{CMC}) curve corresponds to safely measurable absolute values $\tau_y \approx 1-2$ Pa. This indicates that a weak particle network exists even in the presence of a CMC adsorption layer. From the radius of gyration R_g of 153 nm for the CMC used here dissolved in water,[66] we estimate a thickness of the CMC adsorption layer in a similar range, which is not sufficient for a full stabilization of the LiFePO$_4$ particles with $x_{50,3}$ of 2.8 μm. The increase in τ_y upon further addition of CMC is attributed to a depletion attraction among particles induced by the nonadsorbing fraction of CMC molecules freely diffusing in the solvent. This is consistent with the increase in η_∞ observed in the same concentration range as discussed above (see Figure 2A).

FAHP as a particulate secondary polymeric binder was added to the cathode slurries to improve the adhesive strength between the electrode layer and current collector. The rheological properties of these slurries were investigated to understand the influence of FAHP on the flow behavior. Therefore, cathode slurries at a constant ϕ_p of 24 vol % and LiFePO$_4$ to CB volume ratio were characterized at a constant ϕ_{CMC} of 2 vol % but varying FAHP concentrations ϕ_{FAHP}. The chosen CMC concentration corresponds to the critical concentration at which rheological parameters yield a minimum to ensure optimum particle dispersion. Figure 2C displays the yield stress as a function of the FAHP concentration and clearly shows that the addition of the secondary polymer has no effect on particle aggregation. Furthermore, η_∞ is also independent of ϕ_{FAHP} (see the Supporting Information), demonstrating that this polymer added in the form of cross-linked nanoparticles does not affect the flow behavior of the slurry. The contribution of the FAHP

Figure 2. (A) High shear viscosity $\eta_\infty = \eta(\dot{\gamma} = 800\ s^{-1})$ against the CMC concentration of cathode slurries. (B) Yield stress of cathode slurries with/without CB and of CB slurries as a function of ϕ_{CMC}. (C) Yield stress of cathode slurries including CB at a constant ϕ_{CMC} of 2 vol % as a function of ϕ_{FAHP}. LiFePO$_4$ slurries and cathode slurries including LiFePO$_4$ and CB were investigated at a constant ϕ_p of 24 vol % and a constant LiFePO$_4$ to CB mass ratio 48:1. CB slurries were studied at a constant ϕ_p of 3.5 vol %. Note, ϕ_{CMC} and ϕ_{FAHP} refer to the polymer concentration in the dry electrode.

Figure 3. (A) Electrical conductivity of dry cathode layers with and without CB as well as (B) that of CB layers as a function of ϕ_{CMC}. The CMC concentration range in which the corresponding minimum value of τ_y is obtained is marked in red. Lines are drawn to guide the eyes. The standard deviation for conductivity data was determined for three independently prepared samples.
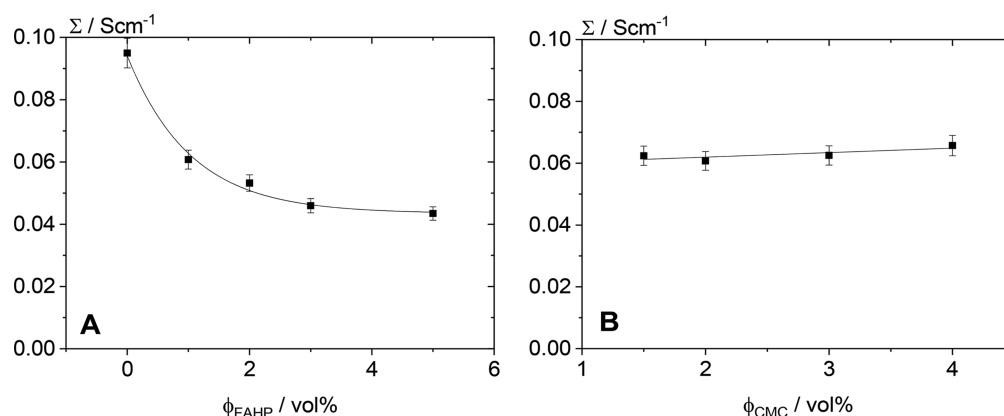
Figure 4. (A) Electrical conductivity of dry cathode layers including CB at a constant ϕ_{CMC} of 2 vol % over ϕ_{FAHP} as well as (B) that of dry cathode layers including CB at a constant ϕ_{FAHP} of 1 vol % as a function of ϕ_{CMC}. The standard deviation for conductivity data was determined for three independently prepared samples.

particles to the overall volume fraction is negligible in comparison to that of the LiFePO$_4$ and CB particles, and moreover, it obviously does not affect the dispersion state of these components. To further confirm this, we prepared cathode slurries with ϕ_{FAHP} of 1 vol % but varying CMC concentrations. Within experimental error, these slurries exhibited the same yield stress as the corresponding slurries without FAHP, and the same is true for the high shear viscosity (see the Supporting Information). These results confirm that FAHP affects neither particle network formation nor the flow behavior of the slurries. These properties are essentially controlled by CMC.

3.2. Electrical Conductivity of Cathode Layers. Particle dispersion in the dry electrode layer strongly affects the electrical conductivity of the electrode and cell resistivity. The electrical conductivity of thin cathode layers made from the slurries investigated above will be discussed next. Figure 3A displays the electrical conductivity of cathode layers with and without CB as a function of ϕ_{CMC}. Cathode layers including CB yield, as expected, overall higher conductivity values than CB-free cathode layers, confirming that the addition of CB is crucial for cathode's electrical conductivity. The electrical conductivity of cathode layers including CB is almost three times higher than for cathode layers made from LFP alone. For cathode layers with or without CB, the electrical conductivity exhibits a maximum with increasing CMC concentration and

decreases at higher ϕ_{CMC}. The CMC concentration at which the maximum conductivity value is reached correlates to the critical concentration at which the minimum τ_y was obtained for corresponding cathode slurries. This clearly confirms that the CMC has a strong impact on particle distribution and the microstructure of the wet slurry as well as the dry cathode layer. A similar effect of a polymeric additive on electrical properties of cathode layers has been observed earlier. Li et al. reported a minimum of the surface resistance upon variation of poly(4-styrene sulfonic acid) (PSSA) concentration in LiFePO$_4$-based layers.[28] This effect was attributed to improved particle distribution due to electrosteric repulsion between particles with adsorbed PSSA. However, the minimum in surface resistance did not systematically correlate to the corresponding rheological findings. Furthermore, it is unclear whether the observed effect on surface resistance is directly caused by PSSA or by further interactions in the cathode slurry since several polymeric additives were used for sample preparation. Interestingly, the maximum value obtained here is nearly twice as high as for optimized layers including specially designed conduction-promoting agents.[27]

The influence of CMC concentration on the electrical conductivity of CB layers is shown in Figure 3B. As expected, the absolute conductivity values are significantly higher than those of cathode layers including LiFePO$_4$. Analogous to layers containing LiFePO$_4$, the electrical conductivity increases with

increasing ϕ_{CMC}, again reaching a maximum at a critical concentration, which correlates to the minimum of τ_y for corresponding CB slurries (see Figure 2B). Higher CMC concentrations lead to a decrease of electrical conductivity since the polymer not adsorbed to the particle surface is randomly distributed in the dry films. This obviously deteriorates and interrupts conductive pathways.

Figure 4A shows the electrical conductivity of dry cathode layers including CB at a constant ϕ_{CMC} of 2 vol % but varying ϕ_{FAHP}. Increasing FAHP concentration leads to a monotonic decrease of the electrical conductivity. Rheological characterization of corresponding cathode slurries did not show a change of yield stress upon variation of ϕ_{FAHP}, i.e., the FAHP particles hardly affect the network of LiFePO$_4$ and CB particles. Consequently, we conclude that the decay in electrical conductivity must be attributed to the randomly distributed FAHP in the dry cathode layer, deteriorating electron transport.

The electrical conductivity of cathode layers including CB and a constant ϕ_{FAHP} of 1 vol % hardly varies with ϕ_{CMC} as displayed in Figure 4B. Irrespective of CMC concentration, the addition of FAHP seems to deteriorate the conductive network. Even though the addition of FAHP exhibits no effect on rheological properties and hence the microstructure of cathode slurries, its presence in the dry layer affects the electrical properties adversely.

3.3. Mechanical Properties of Cathode Layers.
3.3.1. Adhesion. Peel tests performed for pure CMC films on aluminum foil yielded an average line load of 2.8 ± 0.8 N m^{-1}, i.e., the intrinsic contribution of CMC to the adhesive force between the electrode layer and current collector is limited by this value. The effect of polymer addition on the adhesive strength between cathode layers and aluminum foil was also determined using this method.

Figure 5 displays the measured line load of cathode layers as a function of ϕ_{CMC} as well as that of cathode layers including a ϕ_{CMC} of 2 vol % as a function of ϕ_{FAHP}. The line load of samples without FAHP is essentially independent of ϕ_{CMC} and on a technically inacceptable low level around 0.8 N m^{-1}.
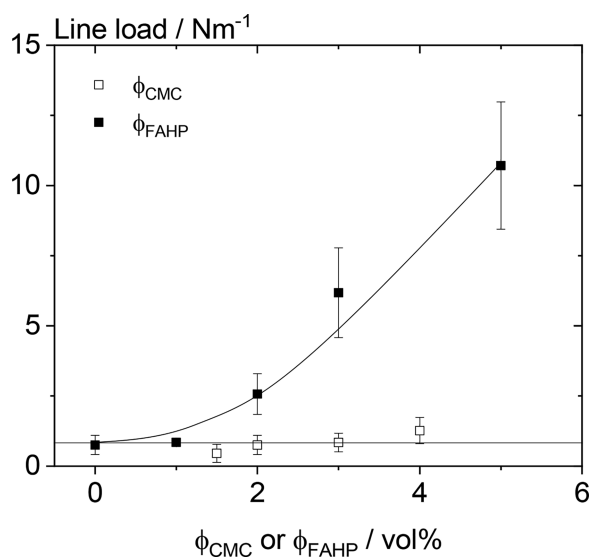

Figure 5. Line load for dry cathode layers without FAHP over ϕ_{CMC} as well as for cathode layers including a constant ϕ_{CMC} of 2 vol % as a function of ϕ_{FAHP}.

Obviously, a second polymer is required to achieve a technically feasible level of adhesion. It should be noted that the presence of CB in the electrode layer has no effect on the line load, irrespective of ϕ_{CMC} (see the Supporting Information).

Here, we have employed FAHP as the secondary polymeric binder. The adhesive strength between pure FAHP films and aluminum foil is characterized by an average line load of 600 ± 50 N m^{-1}, confirming the high potential of FAHP as adhesion promoter for battery electrode layers. As expected, higher ϕ_{FAHP} leads to higher values of the line load, indicating a substantial improvement of the adhesive strength between the layer and current collector. The line load of the investigated samples increases monotonically with increasing ϕ_{FAHP}, reaching over 10 times the value of the reference sample without the secondary polymer at ϕ_{FAHP} of 5 vol %. Nevertheless, this value is still well below the theoretical limit assuming that 5 vol % of the contact area is covered with polymer. The improvement of adhesive strength due to addition of FAHP comes at the cost of the electrical conductivity of the cathode layer (see Figure 4A). A FAHP concentration of 5 vol %, necessary to achieve an adhesive strength of 10 N m^{-1}, results in a drop of electrical conductivity from 0.09 to 0.04 S/cm. However, both electrical conductivity and adhesion strength values still prove to be slightly higher than values reported for similar aqueous LiFePO$_4$-based cathode layers using carboxymethyl/chitosan, CMC/SBR, or xanthan as polymeric binders.[27,30]

3.3.2. Cohesion. Previously, we could show that compressive strength tests on thick anode layers yield reliable and reproducible results, rendering this method suitable for characterization of the cohesive strength of electrode layers. It should be noted that sample porosity has a strong impact on compressive strength. All samples investigated here, however, were confirmed to have a porosity of 60 ± 2%, so this aspect does not need further consideration here.

The cohesive strength of thick cathode layers was determined accordingly, focusing on the effect of the added polymer. The intrinsic mechanical strength of the added polymers was determined by employing tensile tests. Measurements at constant test conditions yield fracture stress values of 35.9 ± 5.2 and 19.6 ± 3.6 N mm^{-2} for FAHP and CMC films, respectively. Figure 6 shows the critical compressive stress at which the sample structure collapses as a function of ϕ_{CMC} for cathode layers with/without CB and as a function of ϕ_{FAHP} for cathode layers including CB and a constant ϕ_{CMC} of 2 vol %. The compressive strength increases almost linearly with increasing ϕ_{CMC} and CB has essentially no effect on the sample failure. This linear relationship apparently does not depend on whether the CMC is adsorbed on the particles or dissolved in the continuous phase of the slurry. Variation of FAHP concentration at a fixed ϕ_{CMC} of 2 vol % also yields a linear relationship between $\sigma_{c,max}$ and polymer concentration. Despite its higher intrinsic mechanical strength, however, the slope of the $\sigma_{c,max}$ vs. ϕ_{FAHP} regression line is only about half that of the $\sigma_{c,max}$ vs. ϕ_{CMC} curve. Furthermore, comparing the data at a given total binder concentration ϕ_{CMC} or ϕ_{CMC} + ϕ_{FAHP} of, e.g., 6 vol % yields an about 50% higher $\sigma_{c,max}$ value for the layer including only CMC as a binder relative to the layer including 2 vol % CMC and 4 vol % FAHP. Obviously, FAHP provides less cohesive strength compared to CMC than theoretically expected. We assume that this is related to the different effects of both binders on the microstructure, i.e., the
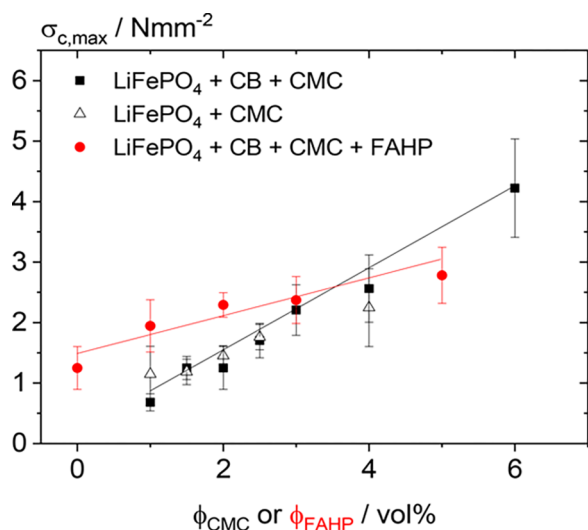
Figure 6. Maximum compressive strength of thick cathode layers with and without CB as a function of ϕ_{CMC} as well as of cathode layers including CB and a ϕ_{CMC} of 2 vol % as a function of ϕ_{FAHP}.

state of dispersion and orientation of the particulate active material. As discussed above, CMC dissolved in the aqueous phase and partly adsorbing on the surface of the LiFePO$_4$ or CB particles has a distinct effect on the microstructure of the slurry, while this is not the case for FAHP (see Figure 2). We hypothesize that CMC also has a strong effect on the structure of the dry electrode layer. This will be discussed in the next section based on image analysis of scanning electron micrographs.

3.3.3. Cathode Microstructure. The porosity of cathode layers including only CMC or a combination of CMC and FAHP as a binder system did not depend on polymer concentration and exhibited values in the range of 58−60% and 60−62%, respectively. SEM images of cathode layers were taken to investigate their microstructure in more detail. Therefore, individual LiFePO$_4$ particles and particle collectives were detected, and their angle of orientation in relation to a centered coordinate system was analyzed. Figure 7A,B shows the SEM micrographs of cathode layers including ϕ_{CMC} of 1.5 and 6 vol %, respectively. The red lines denote the particle orientation in relation to the centered coordinate system marked in white. The particle frequency was then plotted over the angle of orientation for the corresponding cathode layers as shown in Figure 7C,D. Cathodes including low CMC concentration exhibit a random particle orientation, whereas corresponding cathodes with high CMC concentration show a clear particle alignment as indicated by broad and narrow distribution of the particle frequency, respectively. A similar behavior was found for cathode layers including FAHP and CMC as a binder system. Cathode layers with 2 vol % CMC and 5 vol % FAHP exhibit a broad distribution of the particle orientation, indicating an isotropic layer microstructure (Figure 7E). In contrast, samples with a ϕ_{CMC} of 4 vol % and a ϕ_{FAHP} of 1 vol % exhibit a preferred particle orientation of 70−100° (Figure 7F). This aligned microstructure configuration seems to correlate to the high cohesion values obtained for corresponding cathode layers shown in Figure 6.

Compression tests showed a slight increase of cohesive strength when increasing ϕ_{FAHP}. However, the addition of FAHP has no influence on particle orientation (compare Figure 7C and E). We attribute the increment in cohesive

strength upon addition of FAHP to the superior intrinsic mechanical properties of FAHP. However, CMC yields additional cohesive strength through particle alignment in the electrode despite its minor mechanical strength compared to FAHP.

4. CONCLUSIONS

In this study, we comprehensively studied the role of CMC and FAHP as polymeric binders for Li-ion battery cathodes made from water-based slurries of LiFePO$_4$ and CB. The volume fraction of active materials was kept constant and the concentration of CMC and FAHP was systematically varied in a wide range. We investigated not only the effect of these polymers on particle aggregation and flow behavior of the wet slurries but also their impact on electrical conductivity, as well as adhesive and cohesive properties of dry layers and finally also the microstructure of these layers in terms of particle orientation obtained from SEM micrograph image analysis.

Shear rheometry revealed that the yield stress as well as the high shear viscosity exhibits a pronounced minimum at a critical CMC concentration. The decrease of τ_y and η_∞ at low ϕ_{CMC} is attributed to the adsorption of the polymer on the particle surface weakening the particle network present in the slurry due to the electrosteric repulsion partly compensating the strong van der Waals attraction among particles. In this concentration range, CMC improves particle dispersion, but even at the CMC concentration corresponding to the minimum in τ_y and η_∞, a weak percolating particle network exists. At higher CMC concentrations, when particle surfaces are saturated, the polymer dissolved in the continuous, aqueous phase leads to an increase in τ_y presumably caused by attractive depletion interactions among particles and to an increase of η_∞ due to the thickening capacity of the increasing fraction of polymer chains dissolved in the aqueous phase. In contrast to CMC, the FAHP added in the form of cross-linked nanoparticles has no significant effect on active particle dispersion and flow behavior of the slurries, as expected.

Films including CB exhibit a much higher conductivity than those without this additive, emphasizing the prominent role of this additive for the electrical properties of the battery electrodes. However, the electrical conductivity Σ of cathode layers significantly varies with the type and amount of added binder. Upon variation of CMC concentration, Σ exhibits a pronounced maximum at a critical ϕ_{CMC} close to that at which η_∞ and τ_y of the slurry exhibit a minimum, i.e., when the optimum particle dispersion is reached. In contrast, conductivity monotonically decreases with increasing FAHP concentration, probably reaching a limiting value for $\phi_{FAHP} >$ 5 vol %.

As expected from the low intrinsic adhesion of CMC to aluminum, the adhesion of cathode layers including CMC as the only polymeric binder to the current collector is on a technically inacceptable, low level. FAHP, however, has a high affinity to aluminum, and hence, the adhesive strength of cathode layers to the current collector increases monotonically with increasing ϕ_{FAHP}. Absolute values 10 times higher than that without the secondary polymer are reached for $\phi_{FAHP} > 5$ vol %; however, at the expense of a loss in electrical conductivity as discussed above and still, the adhesion is weaker than theoretically expected based on the adhesive strength of the pure polymer.

We have systematically investigated the cohesive strength of cathode layers here for the first time based on compression
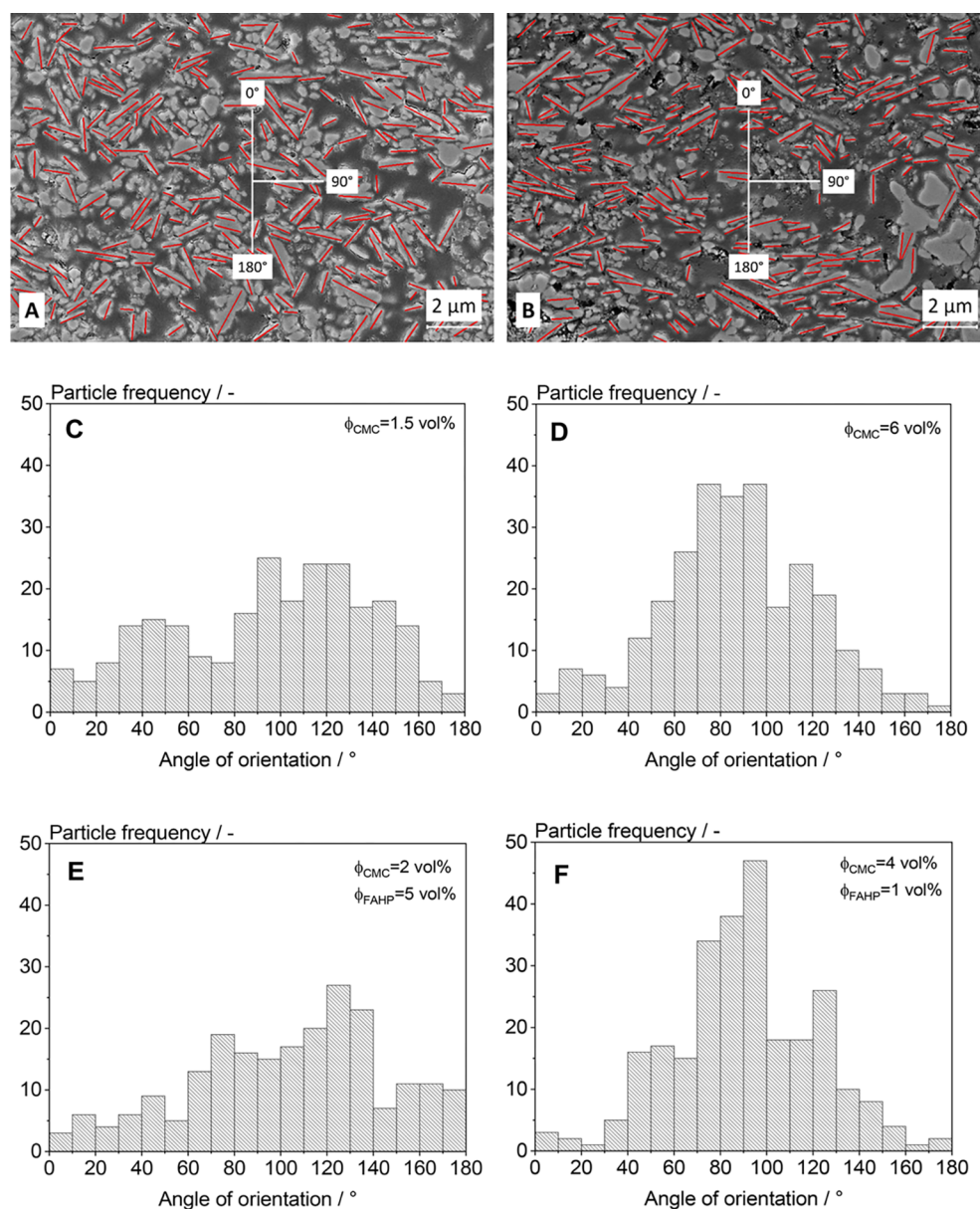
Figure 7. Particle orientation in electrode layers. SEM images of layer including (A) ϕ_{CMC} of 1.5 vol % and (B) ϕ_{CMC} of 6 vol %. Particle frequency as a function of angle of orientation for electrode layers including (C) ϕ_{CMC} of 1.5 vol % and ϕ_{FAHP} of 0 vol %, (D) ϕ_{CMC} of 6 vol % and ϕ_{FAHP} of 0 vol %, (E) ϕ_{CMC} of 2 vol % and ϕ_{FAHP} of 5 vol %, and (F) ϕ_{CMC} of 4 vol % and ϕ_{FAHP} of 1 vol %.

tests performed on thick films with similar porosity and microstructure as the thin cathode layers. Compressive strength increases linearly with increasing ϕ_{CMC} or ϕ_{FAHP}. Despite its lower intrinsic cohesive strength, this increase in cathode layer cohesion is more pronounced with added CMC than with FAHP. Microstructural investigations based on image analysis of SEM micrographs revealed that CMC has a strong effect on particle orientation with pronounced particle alignment at high ϕ_{CMC}. On the other hand, a random particle orientation is found when FAHP is added, irrespective of concentration. These different impacts of the investigated polymers on the microstructure and particle orientation seem to be the origin of the strong contribution of CMC to the cohesive strength of the cathode layers.

■ ASSOCIATED CONTENT

Ⓢ Supporting Information

The Supporting Information is available free of charge at

https://pubs.acs.org/doi/10.1021/acsomega.0c00477.

Viscosity as a function of shear rate for cathode slurries including different CMC concentrations. High shear viscosity as a function of FAHP concentration for cathode slurries including 2 vol % CMC. High shear viscosity and yield stress as a function of CMC concentration for cathode slurries with and without FAHP. Line load of dry cathode layers with and without CB as a function of CMC concentration (PDF)

■ AUTHOR INFORMATION

Corresponding Author

    Ronald Gordon − *Karlsruhe Institute of Technology (KIT), Institute of Mechanical Process Engineering and Mechanics − Applied Mechanics Group, Karlsruhe D-76131, Germany;* orcid.org/0000-0002-3541-9018; Phone: +49 721 608-43757; Email: ronald.gordon@kit.edu; Fax: +49 721 608-43758

Authors

    Meriem Kassar − *Karlsruhe Institute of Technology (KIT), Institute of Mechanical Process Engineering and Mechanics − Applied Mechanics Group, Karlsruhe D-76131, Germany*

    Norbert Willenbacher − *Karlsruhe Institute of Technology (KIT), Institute of Mechanical Process Engineering and Mechanics − Applied Mechanics Group, Karlsruhe D-76131, Germany*

Complete contact information is available at:
https://pubs.acs.org/10.1021/acsomega.0c00477

Author Contributions

The manuscript was written through contributions of all authors. All authors have given approval to the final version of the manuscript. These authors contributed as follows: R.G. contributed in the conceptualization, methodology, formal analysis, investigation, writing the original draft, and visualization, M.K. in the methodology, formal analysis, and investigation, and N.W. in writing − review and editing and supervision.

Notes

The authors declare no competing financial interest.

■ ABBREVIATIONS

CMC, carboxymethyl cellulose; FAHP, fluorine/acrylate hybrid polymer; LiB, lithium-ion battery; LFP, lithium iron phosphate; CB, carbon black; NMP, *N*-methyl-2-pyrrolidone; PAA, polyacrylic acid; CTS, chitosan; CCTS, carboxymethyl/chitosan; CN-CCTS, cyanoethylated carboxymethyl chitosan; PSSA, poly(4-sterene sulfonic acid); SBR, styrene butadiene rubber; PVAc, poly(vinyl acetate); PTFE, polytetrafluoroethylene

■ REFERENCES

(1) Padhi, A. K. Phospho-Olivines as Positive-Electrode Materials for Rechargeable Lithium Batteries. *J. Electrochem. Soc.* **1997**, *144*, 1188.

(2) Yamada, A.; Chung, S. C.; Hinokuma, K. Optimized LiFePO[Sub 4] for Lithium Battery Cathodes. *J. Electrochem. Soc.* **2001**, *148*, A224.

(3) MacNeil, D. D.; Lu, Z.; Chen, Z.; Dahn, J. R. A Comparison of the Electrode/Electrolyte Reaction at Elevated Temperatures for Various Li-Ion Battery Cathodes. *J. Power Sources* **2002**, *108*, 8−14.

(4) Iltchev, N.; Chen, Y.; Okada, S.; Yamaki, J. I. LiFePO4 Storage at Room and Elevated Temperatures. *J. Power Sources* **2003**, *119-121*, 749−754.

(5) Striebel, K.; Shim, J.; Srinivasan, V.; Newman, J. Comparison of LiFePO[Sub 4] from Different Sources. *J. Electrochem. Soc.* **2005**, *152*, A664.

(6) Zhang, W. J. Structure and Performance of LiFePO4 Cathode Materials: A Review. *J. Power Sources* **2011**, *196*, 2962−2970.

(7) Andersson, A. S.; Thomas, J. O. The Source of First-Cycle Capacity Loss in LiFePO₄. *J. Power Sources* **2001**, *97-98*, 498−502.

(8) Prosini, P. P.; Cento, C.; Carewska, M.; Masci, A. Electrochemical Performance of Li-Ion Batteries Assembled with Water-Processable Electrodes. *Solid State Ionics* **2015**, *274*, 34−39.

(9) Wang, C.; Hong, J. Ionic/Electronic Conducting Characteristics of LiFePO₄ Cathode Materials. *Electrochem. Solid-State Lett.* **2007**, *10*, A65.

(10) Huang, H.; Yin, S.-C.; Nazar, L. F. Approaching Theoretical Capacity of LiFePO₄ at Room Temperature at High Rates. *Electrochem. Solid-State Lett.* **2001**, *4*, A170.

(11) Chung, S. Y.; Bloking, J. T.; Chiang, Y. M. Electronically Conductive Phospho-Olivines as Lithium Storage Electrodes. *Nat. Mater.* **2002**, *1*, 123−128.

(12) Croce, F.; D'Epifanio, A.; Hassoun, J.; Deptula, A.; Olczac, T.; Scrosati, B. A Novel Concept for the Synthesis of an Improved LiFePO[Sub 4] Lithium Battery Cathode. *Electrochem. Solid-State Lett.* **2002**, *5*, A47.

(13) Chung, S.-Y.; Chiang, Y.-M. Microscale Measurements of the Electrical Conductivity of Doped LiFePO₄. *Electrochem. Solid-State Lett.* **2003**, *6*, A278.

(14) Herle, P. S.; Ellis, B.; Coombs, N.; Nazar, L. F. Nano-Network Electronic Conduction in Iron and Nickel Olivine Phosphates. *Nat. Mater.* **2004**, *3*, 147−152.

(15) Delacourt, C.; Poizot, P.; Levasseur, S.; Masquelier, C. Size Effects on Carbon-Free LiFePO₄ Powders. *Electrochem. Solid-State Lett.* **2006**, *9*, A352.

(16) Hu, Y. S.; Guo, Y. G.; Dominko, R.; Gaberscek, M.; Jamnik, J.; Maier, J. Improved Electrode Performance of Porous LiFePO₄ Using RuO₂ as an Oxidic Nanoscale Interconnect. *Adv. Mater.* **2007**, *19*, 1963−1966.

(17) Qi, X.; Blizanac, B.; Dupasquier, A.; Oljaca, M.; Li, J.; Winter, M. Understanding the Influence of Conductive Carbon Additives Surface Area on the Rate Performance of LiFePO₄ Cathodes for Lithium Ion Batteries. *Carbon N. Y.* **2013**, *64*, 334−340.

(18) Zheng, H.; Li, J.; Song, X.; Liu, G.; Battaglia, V. S. A Comprehensive Understanding of Electrode Thickness Effects on the Electrochemical Performances of Li-Ion Battery Cathodes. *Electrochim. Acta* **2012**, *71*, 258−265.

(19) Nguyen, V. H.; Wang, W. L.; Jin, E. M.; Gu, H. B. Impacts of Different Polymer Binders on Electrochemical Properties of LiFePO₄ Cathode. *Appl. Surf. Sci.* **2013**, *282*, 444−449.

(20) Bauer, W.; Nötzel, D. Rheological Properties and Stability of NMP Based Cathode Slurries for Lithium Ion Batteries. *Ceram. Int.* **2014**, *40*, 4591−4598.

(21) Cai, Z. P.; Liang, Y.; Li, W. S.; Xing, L. D.; Liao, Y. H. Preparation and performances of LiFePO₄ cathode in aqueous solvent with polyacrylic acid as a binder. *J. Power Sources* **2009**, *189*, 547−551.

(22) Chong, J.; Xun, S.; Zheng, H.; Song, X.; Liu, G.; Ridgway, P.; Wang, J. Q.; Battaglia, V. S. A Comparative Study of Polyacrylic Acid and Poly(Vinylidene Difluoride) Binders for Spherical Natural Graphite/LiFePO₄ Electrodes and Cells. *J. Power Sources* **2011**, *196*, 7707−7714.

(23) Zhang, Z.; Zeng, T.; Qu, C.; Lu, H.; Jia, M.; Lai, Y.; Li, J. Cycle Performance Improvement of LiFePO₄ Cathode with Polyacrylic Acid as Binder. *Electrochim. Acta* **2012**, *80*, 440−444.

(24) Sun, M.; Zhong, H.; Jiao, S.; Shao, H.; Zhang, L. Investigation on Carboxymethyl Chitosan as New Water Soluble Binder for LiFePO₄ Cathode in Li-Ion Batteries. *Electrochim. Acta* **2014**, *127*, 239−244.

(25) He, J.; Wang, J.; Zhong, H.; Ding, J.; Zhang, L. Cyanoethylated Carboxymethyl Chitosan as Water Soluble Binder with Enhanced Adhesion Capability and Electrochemical Performances for LiFePO₄ Cathode. *Electrochim. Acta* **2015**, *182*, 900−907.

(26) Prasanna, K.; Subburaj, T.; Jo, Y. N.; Lee, W. J.; Lee, C. W. Environment-Friendly Cathodes Using Biopolymer Chitosan with Enhanced Electrochemical Behavior for Use in Lithium Ion Batteries. *ACS Appl. Mater. Interfaces* **2015**, *7*, 7884−7890.

(27) Zhong, H.; He, A.; Lu, J.; Sun, M.; He, J.; Zhang, L. Carboxymethyl Chitosan/Conducting Polymer as Water-Soluble Composite Binder for LiFePO₄ cathode in Lithium Ion Batteries. *J. Power Sources* **2016**, *336*, 107−114.

(28) Li, C.-C.; Peng, X.-W.; Lee, J.-T.; Wang, F.-M. Using Poly(4-Styrene Sulfonic Acid) to Improve the Dispersion Homogeneity of Aqueous-Processed LiFePO₄ Cathodes. *J. Electrochem. Soc.* **2010**, *157*, A517.

(29) Gao, S.; Su, Y.; Bao, L.; Li, N.; Chen, L.; Zheng, Y.; Tian, J.; Li, J.; Chen, S.; Wu, F. High-Performance LiFePO₄/C Electrode with Polytetrafluoroethylene as an Aqueous-Based Binder. *J. Power Sources* **2015**, *298*, 292−298.

(30) He, J.; Zhong, H.; Wang, J.; Zhang, L. Investigation on xanthan gum as novel water soluble binder for LiFePO₄ cathode in lithium-ion batteries. *J. Alloys Compd.* **2017**, *714*, 409−418.

(31) Lee, J.-H.; Kim, J.-S.; Kim, Y. C.; Zang, D. S.; Choi, Y.-M.; Park, W. I.; Paik, U. Effect of Carboxymethyl Cellulose on Aqueous Processing of LiFePO₄ Cathodes and Their Electrochemical Performance. *Electrochem. Solid-State Lett.* **2008**, *11*, A175.

(32) Porcher, W.; Moreau, P.; Lestriez, B.; Jouanneau, S.; Guyomard, D. Is LiFePO₄ Stable in Water? *Electrochem. Solid-State Lett.* **2008**, *11*, A4.

(33) Porcher, W.; Lestriez, B.; Jouanneau, S.; Guyomard, D. Design of Aqueous Processed Thick LiFePO₄ Composite Electrodes for High-Energy Lithium Battery. *J. Electrochem. Soc.* **2009**, *156*, A133.

(34) Lux, S. F.; Schappacher, F.; Balducci, A.; Passerini, S.; Winter, M. Low Cost, Environmentally Benign Binders for Lithium-Ion Batteries. *J. Electrochem. Soc.* **2010**, *157*, A320.

(35) Kim, G. T.; Jeong, S. S.; Joost, M.; Rocca, E.; Winter, M.; Passerini, S.; Balducci, A. Use of Natural Binders and Ionic Liquid Electrolytes for Greener and Safer Lithium-Ion Batteries. *J. Power Sources* **2011**, *196*, 2187−2194.

(36) Li, C.-C.; Lin, Y.-S. Interactions between Organic Additives and Active Powders in Water-Based Lithium Iron Phosphate Electrode Slurries. *J. Power Sources* **2012**, *220*, 413−421.

(37) Qiu, L.; Shao, Z.; Wang, D.; Wang, F.; Wang, W.; Wang, J. Novel Polymer Li-Ion Binder Carboxymethyl Cellulose Derivative Enhanced Electrochemical Performance for Li-Ion Batteries. *Carbohydr. Polym.* **2014**, *112*, 532−538.

(38) Tsai, F. Y.; Jhang, J. H.; Hsieh, H. W.; Li, C. C. Dispersion, Agglomeration, and Gelation of LiFePO₄ in Water-Based Slurry. *J. Power Sources* **2016**, *310*, 47−53.

(39) Wu, Q.; Ha, S.; Prakash, J.; Dees, D. W.; Lu, W. Investigations on High Energy Lithium-Ion Batteries with Aqueous Binder. *Electrochim. Acta* **2013**, *114*, 1−6.

(40) Çetinel, F. A.; Bauer, W. Processing of Water-Based LiNi1/3Mn1/3Co1/3O2 Pastes for Manufacturing Lithium Ion Battery Cathodes. *Bull. Mater. Sci.* **2014**, *37*, 1685−1690.

(41) Notake, K.; Gunji, T.; Kokubun, H.; Kosemura, S.; Mochizuki, Y.; Tanabe, T.; Kaneko, S.; Ugawa, S.; Lee, H.; Matsumoto, F. The Application of a Water-Based Hybrid Polymer Binder to a High-Voltage and High-Capacity Li-Rich Solid-Solution Cathode and Its Performance in Li-Ion Batteries. *J. Appl. Electrochem.* **2016**, *46*, 267−278.

(42) Tanabe, T.; Gunji, T.; Honma, Y.; Miyamoto, K.; Tsuda, T.; Mochizuki, Y.; Kaneko, S.; Ugawa, S.; Lee, H.; Ohsaka, T.; Matsumoto, F. Preparation of Water-Resistant Surface Coated High-Voltage LiNi0.5Mn1.5O4 Cathode and Its Cathode Performance to Apply a Water-Based Hybrid Polymer Binder to Li-Ion Batteries. *Electrochim. Acta* **2017**, *224*, 429−438.

(43) Kazzazi, A.; Bresser, D.; Birrozzi, A.; Von Zamory, J.; Hekmatfar, M.; Passerini, S. Comparative Analysis of Aqueous Binders for High-Energy Li-Rich NMC as a Lithium-Ion Cathode and the Impact of Adding Phosphoric Acid. *ACS Appl. Mater. Interfaces* **2018**, *10*, 17214−17222.

(44) Dominko, R.; Gaberscek, M.; Drofenik, J.; Bele, M.; Pejovnik, S.; Jamnik, J. The Role of Carbon Black Distribution in Cathodes for Li Ion Batteries. *J. Power Sources* **2003**, *119-121*, 770−773.

(45) Guy, D.; Lestriez, B.; Bouchet, R.; Guyomard, D. Critical Role of Polymeric Binders on the Electronic Transport Properties of Composites Electrode. *J. Electrochem. Soc.* **2006**, *153*, A679.

(46) Lestriez, B. Functions of Polymers in Composite Electrodes of Lithium Ion Batteries. *Comptes Rendus Chim.* **2010**, *13*, 1341−1350.

(47) Liu, G.; Zheng, H.; Song, X.; Battaglia, V. S. Particles and Polymer Binder Interaction: A Controlling Factor in Lithium-Ion Electrode Performance. *J. Electrochem. Soc.* **2012**, *159*, A214−A221.

(48) Arora, P. Capacity Fade Mechanisms and Side Reactions in Lithium-Ion Batteries. *J. Electrochem. Soc.* **1998**, *145*, 3647.

(49) Rahani, E. K.; Shenoy, V. B. Role of Plastic Deformation of Binder on Stress Evolution during Charging and Discharging in Lithium-Ion Battery Negative Electrodes. *J. Electrochem. Soc.* **2013**, *160*, A1153−A1162.

(50) Son, B.; Ryou, M. H.; Choi, J.; Lee, T.; Yu, H. K.; Kim, J. H.; Lee, Y. M. Measurement and Analysis of Adhesion Property of Lithium-Ion Battery Electrodes with SAICAS. *ACS Appl. Mater. Interfaces* **2014**, *6*, 526−531.

(51) Zhang, Z.; Zeng, T.; Lai, Y.; Jia, M.; Li, J. A comparative study of different binders and their effects on electrochemical properties of LiMn₂O₄ cathode in lithium ion batteries. *J. Power Sources* **2014**, *247*, 1−8.

(52) Haselrieder, W.; Westphal, B.; Bockholt, H.; Diener, A.; Höft, S.; Kwade, A. Measuring the Coating Adhesion Strength of Electrodes for Lithium-Ion Batteries. *Int. J. Adhes. Adhes.* **2015**, *60*, 1−8.

(53) Kim, K.; Byun, S.; Cho, I.; Ryou, M. H.; Lee, Y. M. Three-Dimensional Adhesion Map Based on Surface and Interfacial Cutting Analysis System for Predicting Adhesion Properties of Composite Electrodes. *ACS Appl. Mater. Interfaces* **2016**, *8*, 23688−23695.

(54) Gaikwad, A. M.; Arias, A. C. Understanding the Effects of Electrode Formulation on the Mechanical Strength of Composite Electrodes for Flexible Batteries. *ACS Appl. Mater. Interfaces* **2017**, *9*, 6390−6400.

(55) Babinec, S.; Tang, H.; Talik, A.; Hughes, S.; Meyers, G. Composite Cathode Structure/Property Relationships. *J. Power Sources* **2007**, *174*, 508−514.

(56) Zheng, H.; Zhang, L.; Liu, G.; Song, X.; Battaglia, V. S. Correlationship between Electrode Mechanics and Long-Term Cycling Performance for Graphite Anode in Lithium Ion Cells. *J. Power Sources* **2012**, *217*, 530−537.

(57) Lee, B. R.; Oh, E. S. Effect of Molecular Weight and Degree of Substitution of a Sodium-Carboxymethyl Cellulose Binder on Li₄Ti₅O₁₂ anodic Performance. *J. Phys. Chem. C* **2013**, *117*, 4404−4409.

(58) Wu, M.; Xiao, X.; Vukmirovic, N.; Xun, S.; Das, P. K.; Song, X.; Olalde-Velasco, P.; Wang, D.; Weber, A. Z.; Wang, L. W.; Battaglia, V. S.; Yang, W.; Liu, G. Toward an Ideal Polymer Binder Design for High-Capacity Battery Anodes. *J. Am. Chem. Soc.* **2013**, *135*, 12048−12056.

(59) Chen, J.; Liu, J.; Qi, Y.; Sun, T.; Li, X. Unveiling the Roles of Binder in the Mechanical Integrity of Electrodes for Lithium-Ion Batteries. *J. Electrochem. Soc.* **2013**, *160*, A1502−A1509.

(60) Antartis, D.; Dillon, S.; Chasiotis, I. Effect of Porosity on Electrochemical and Mechanical Properties of Composite Li-Ion Anodes. *J. Compos. Mater.* **2015**, *49*, 1849−1862.

(61) Hernandez, C. R.; Etiemble, A.; Douillard, T.; Mazouzi, D.; Karkar, Z.; Maire, E.; Guyomard, D.; Lestriez, B.; Roué, L. A Facile and Very Effective Method to Enhance the Mechanical Strength and the Cyclability of Si-Based Electrodes for Li-Ion Batteries. *Adv. Energy Mater.* **2018**, *8*, 1701787.

(62) Barnes, H. A.; Carnali, J. O. The Vane-in-cup as a Novel Rheometer Geometry for Shear Thinning and Thixotropic Materials. *J. Rheol.* **1990**, *34*, 841−866.

(63) Yüce, C.; Willenbacher, N. Challenges in Rheological Characterization of Highly Concentrated Suspensions - A Case

Study for Screen-Printing Silver Pastes. *J. Visualized Exp.* **2017**, *122*, 1−17.

(64) Smits, F. M. Measurement of Sheet Resistivities with the Four-Point Probe. *Bell Syst. Tech. J.* **1958**, *37*, 711−718.

(65) Lim, S.; Kim, S.; Ahn, K. H.; Lee, S. J. The Effect of Binders on the Rheological Properties and the Microstructure Formation of Lithium-Ion Battery Anode Slurries. *J. Power Sources* **2015**, *299*, 221−230.

(66) Chatterjee, A.; Das, B. Radii of Gyration of Sodium Carboxymethylcellulose in Aqueous and Mixed Solvent Media from Viscosity Measurement. *Carbohydr. Polym.* **2013**, *98*, 1297−1303.